IET Power Electronics

Research Article

IET Journals
The Institution of Engineering and Technology

Discrete-time integral terminal sliding mode based maximum power point controller for the PMSG-based wind energy system

ISSN 1755-4535
Received on 22nd January 2019
Revised 21st June 2019
Accepted on 5th August 2019
E-First on 24th October 2019
doi: 10.1049/iet-pel.2019.0106
www.ietdl.org

İrfan Yazıcı[1], Ersagun Kürşat Yaylacı[2] ✉

[1]*Department of Electrical and Electronics Engineering, Sakarya University, Sakarya 54050, Turkey*
[2]*Department of Electrical and Electronics Engineering, Karabuk University, Karabuk 78050, Turkey*
✉ *E-mail: ekyaylaci@karabuk.edu.tr*

Abstract: This study proposes a discrete-time integral terminal sliding mode controller (DITSMC) integrated with a sensorless maximum power point tracking (MPPT) method for a permanent magnet synchronous generator (PMSG)-based wind energy conversion system (WECS). The effects of the parameters of the proposed DITSMC on the convergence-time and the error-bound are investigated by the simulation studies. The dynamic performance of the DITSMC has been evaluated experimentally on a test bench for step-type wind changes. The optimum coefficient between the output voltage of the generator and the extracted power from the WECS is determined only for a wind speed by offline studies. Then, the MPPT can be provided using this coefficient for all wind speeds in the operating range of the WECS without any mechanical sensor. Additionally, the experimental studies show that DITSMC has better performance than the PI controller in terms of the settling time and thus the efficiency of the WECS.

1 Introduction

Renewable energy sources have great attention compared to the conventional energy sources due to the increasing environmental concerns such as global warming effect and fossil fuel pollution. One of the renewable energy sources is the wind energy which has the largest market share and rapidly grown for the future [1]. For the near future, the wind energy source might be the most cost-effective energy source according to the exploited sources with the incentives and financial supports of the governments all over the world [2].

Although the Wind Energy Conversion System (WECS) is operated at the variable speed or fixed speed, the maximisation of the power captured from the wind is only assured with the variable speed operation. Also, the variable speed WECS is the most preferred one, thanks to the higher power quality and lower mechanical stresses [3, 4]. It is shown that the variable speed WECS with the maximum power point tracking (MPPT) capability has a higher energy output ∼10–15% than the fixed speed WECS [5].

The different generator types such as double-fed induction generator and permanent magnet synchronous generator (PMSG) are used in variable speed WECS. The PMSGs can be preferred in both low and high power applications [6]. In this study, a PMSG-based WECS is used.

In the literature, many various kinds of methods have been offered to provide MPPT for the WECS. The MPPT methods provide only the knowledge of the operating points that the system can give maximum power. These points are called as the maximum power point (MPP). Therefore, a controller is needed to bring the WECS to the MPP appointed by the MPPT methods. Thus, another important issue is the controller design to obtain an efficient WECS. Some expectations from the controller used for MPPT in the WECS can be given as follows:

i. Considering the rapidly changing wind conditions, the controller should bring the system to the reference value estimated by the MPPT method with the minimum steady-state error as soon as possible.
ii. The controller should have a satisfying performance over a wide range of wind speed.

In recent years, many studies have been presented to design a controller for the WECS in the literature. Considering the wide range of the operating points and highly non-linear behaviours of the WECS, classical linear controllers did not have sufficient performances [7]. Therefore, the performances of the PI/PID controllers were supported with the intelligent control approaches such as a fuzzy logic controller, particle swarm optimisation [8–11].

The sliding mode control (SMC) method that is one of the non-linear control methods was also offered for the WECS [12–16]. In [12], the tip-to-speed ratio (TSR)-based MPPT method with the sliding mode (SM) torque controller and the power signal feedback (PSF)-based MPPT method with the high-order SMC were suggested. In [13], an SM-based control method integrated with the PSO was offered. In [14], an integral SMC was offered to track an optimal reference value produced by the fuzzy logic controller.

The SMC is a robust control method in terms of the parametric uncertainties, external disturbances, and parameter variations if the system trajectories are in the SM [17–20]. Moreover, the SMC method has an easy implementation capability for any system compared to the other nonlinear control methods [21]. The main drawbacks of the conventional SMC are a steady-state error in the regulation, and high-frequency chattering resulted from the switching action in real-time applications [22, 23]. To eliminate the steady-state error in conventional SMC, an additional integral term of the state variable is introduced to the sliding surface and thus the SMC structure known as integral SMC (ISMC) is obtained. Also, ISMC has a lower chattering for any system than SMC [24]. The other drawback of the conventional SMC is that it has infinite settling time due to its asymptotic structure [25]. Therefore, a new type of SMC called terminal SMC (TSMC) was offered to provide finite-time convergence stability [26]. Also, the TSMC can improve transient performance of the system as compared with the conventional SMC [27].

In most of the ISMC and the TSMC applications, the controller designs were on the continuous-time basis [28–30]. However, in real-time applications, controllers are generally realised by a digital processor with finite sampling rate. Hence, the discrete-time design of the existing continuous-time ITSMC (ITSMC) for the wind energy systems is worth considering.

The main aim of this study is to develop a discrete-time ITSMC (DITSMC)-based MPPT structure in order to increase the energy

efficiency of a WECS by decreasing the convergence-time and the error-bound. The proposed DITSMC-based approach is newly introduced to the literature [31] and its performance is not yet investigated on a WECS. Therefore, the proposed study will contribute to the literature as the first study in which DITSMC is applied to WECSs. Also, the effects of the design parameters of the proposed DITSMC on the convergence-time and the error-bounds are investigated by the simulation studies. The dynamic performance of the proposed DITSMC is shown by the experiments on a test bench for various wind conditions. Additionally, experimental studies show that the proposed DITSMC has better performance than the proportional–integral (PI) controller in terms of the settling time and thus the efficiency of the WECS. However, only the results of some experiments are given, taking into account the length of the paper.

In this study, the optimum coefficient between the output voltage of the PMSG and the extracted power from the WECS is obtained for only one wind speed by the offline studies. After that, the obtained coefficient can be used to get the MPPT reference value without any mechanical sensor. The elimination of the mechanical sensor requirement is particularly important for small WECS due to the system cost.

This paper is presented as follows. The WECS configurations are explained in Section 2. The controller design, experimental results, and conclusion are presented in Section 3–5, respectively.

2 WECS configurations

The block diagram of the WECS used in this paper is given in Fig. 1. The PMSG coupled directly to the wind turbine (WT) is widely used for the WECS. The output of the PMSG is connected to the load by a three-phase uncontrolled rectifier and a boost converter (BC). The MPPT is assured by changing the duty ratio of the BC via a controller.

2.1 WT characteristics

Mechanical power extracted from the wind can be given as

$$P_m = 0.5\rho\pi R^2 c_p V_{\mathrm{w}}^3 \tag{1}$$

where ρ is the air density (kg/m^3), c_{P} is the performance coefficient, V_{w} is the wind speed (m/s), R is the rotor radius (m). The output power of the turbine can be maximised when the performance coefficient (c_p), depending on the blade pitch angle (β) and TSR (λ) of the turbine, is maximised. In other words, the value of the c_p indicates how much the system comes close to the MPP. In this study, the model which is widely preferred in the literature and introduced in detail in [32] is used

$$c_p(\lambda,\beta) = 0.5176\left(\left(\frac{1}{\lambda+0.08\beta}-\frac{0.035}{\beta^3+1}\right)116\right)x \\ -0.4\beta-5 \\ \mathrm{e}^{\left(\left(0.735/(\beta^3+1)\right)-\left(21/(\lambda+0.08\beta)\right)\right)}+0.0068\lambda \tag{2}$$

The TSR (λ) is described as follows [33]:

$$\lambda = \frac{\omega_m R}{V_{\mathrm{w}}} \tag{3}$$

where ω_m is the rotational speed of the blades (rad/s). The c_p–λ curve of the WT generated by using the MATLAB is shown in Fig. 2*a* for $\beta = 0$. From Fig. 2*a*, it can be concluded that the WT has only one optimal TSR value to get maximum performance coefficient and thus the maximum power. The optimal value of the TSR can be determined by the experiment or the theoretical studies. The c_p curve of the established test bench, which will be explained in detail in Section 4, is also given in Fig. 2*b*. The upper value of the rotational speed (ω_{up}) of the system is limited to avoid any failure. Fig. 2*b* shows the real-time c_p curve of the test bench for $\omega_{\mathrm{up}} = 500$, 550 and 600 rpm.

2.2 Electrical characteristics

In order to extract the maximum power from the WECS, the rotational speed of the PMSG can be controlled easily by changing the duty ratio of the BC as shown in Fig. 1.

The following expressions can be presented for the WECS given in Fig. 1. The phase-back electromotive force (E) is proportional to the generator speed ω_m as

$$E = k_{\mathrm{e}}\omega_m \tag{4}$$

where k_{e} is the electromotive force coefficient of the PMSG.

The rectified DC voltage V_{in} at the input of the BC can be given as [34]

$$V_{\mathrm{in}} = \frac{3\sqrt{6}}{\pi}\left(E-\frac{\sqrt{6}}{6}k_m\omega_m\right) = \frac{3\sqrt{6}}{\pi}\left(k_{\mathrm{e}}-\frac{\sqrt{6}}{6}k_m\right)\omega_m \tag{5}$$

where k_{m} denotes the electrical constant of the three-phase uncontrolled bridge rectifier.

2.3 Used MPPT method

As stated in Section 1, there are various types of MPPT methods in the literature. The MPPT methods have not been given here since they are reviewed in detail in the literature. Only the used MPPT method is summarised briefly as below.

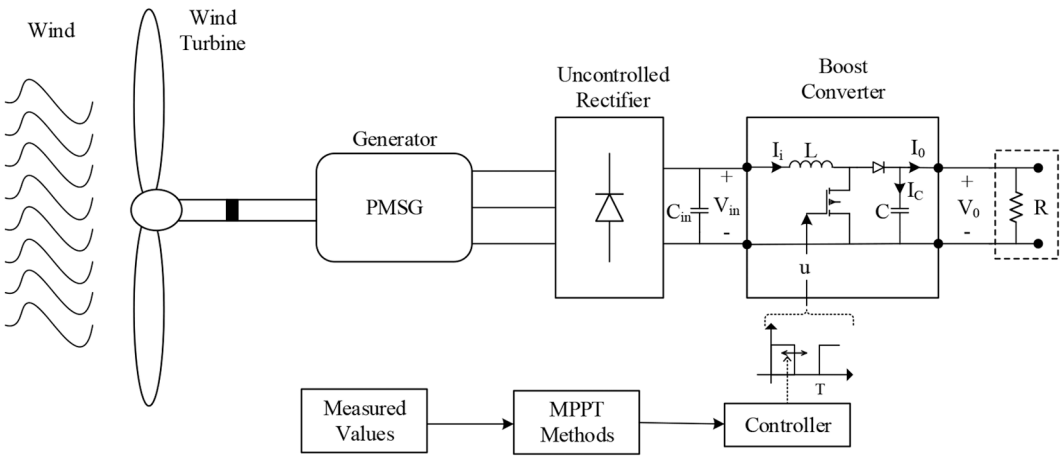

Fig. 1 *Block diagram of the WECS*

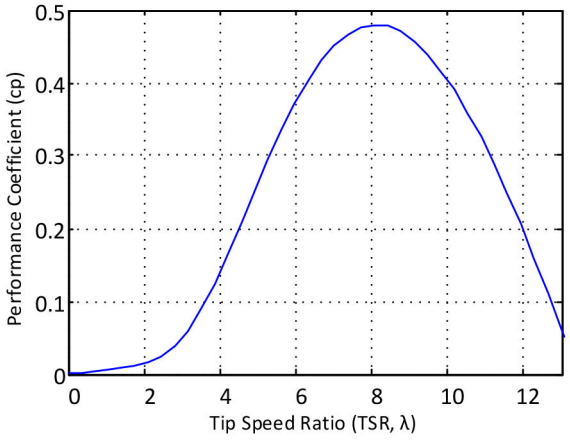

a

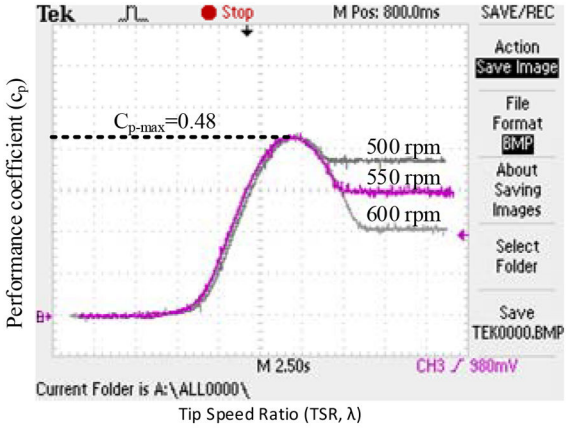

b

Fig. 2 *c_p–TSR curve for the WT*

(a) In the simulation, ***(b)*** In the test bench

The PSF method is one of the MPPT methods and uses the relationship between the rotational speed and the extracted maximum mechanical power from the WECS as given below [35]:

$$P_{m-\max} = k_{\text{opt}}\omega_m^3 \tag{6}$$

where

$$k_{\text{opt}} = \frac{0.5\rho\pi R^5 c_{p-\max}}{\lambda_{\text{opt}}^3} \tag{7}$$

The k_{opt} is the optimal speed coefficient provided only when the TSR is at its own optimal value. As can be seen from (5), the rectified dc voltage of the PMSG is directly proportional to the rotational speed. Therefore, V_{in} can be replaced by the ω_m in (6). The relationship between V_{in} and ω_m obtained for the test bench used in this paper is shown in Fig. 3.

Neglecting the efficiencies of the generator, rectifier and converter, the maximum-electrical power delivered to the load ($P_{L\text{-}\max}$) can be expressed as follows:

$$P_{L-\max} = k_{v-\text{opt}}V_{\text{in}-\text{opt}}^3 \tag{8}$$

where $k_{v-\text{opt}}$ is the optimum voltage coefficient to get MPPT. The maximum power can be obtained by tracking the $V_{\text{in-opt}}$ due to the fact that the V_{in} directly affects the load power [14]. The schematic block diagram of the used MPPT method is given in Fig. 4. For more detail about the used method [14, 36] can be examined. It is enough to find the $k_{v-\text{opt}}$ for only one wind speed because its value is approximately constant for every wind speed. It can be concluded that the MPPT can be assured approximately by using this coefficient.

3 Controller design

The behavioural model of the BC used in the WECS shown in Fig. 1 can be defined by the following equations:

$$\frac{\mathrm{d}I_{\text{in}}}{\mathrm{d}t} = \frac{1}{L}(V_{\text{in}} - V_{\text{o}}\bar{u}) \tag{9a}$$

$$\frac{\mathrm{d}V_{\text{o}}}{\mathrm{d}t} = \frac{1}{C}\left(I_{\text{in}}\bar{u} - \frac{V_{\text{o}}}{R}\right) \tag{9b}$$

$$V_{\text{in}} = \alpha V_{\text{o}} \tag{9c}$$

where L is the boost inductance, C is the output capacitor, $u = [0, 1]$ logic switching control signal, $\bar{u} = 1 - u$: inverse logic of u, R is the output resistance and α denotes the converter ratio.

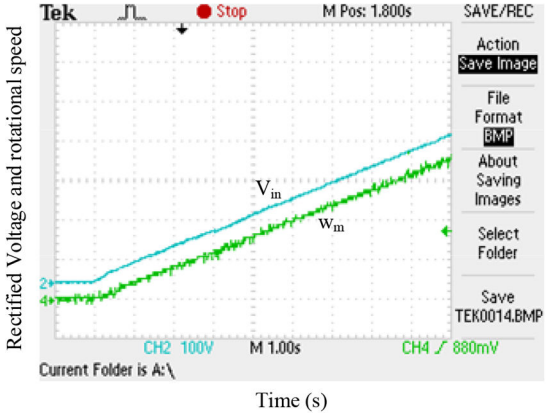

Fig. 3 *Relationship between V_{in} and ω_m*

V_{in}, I_{in} and V_{o} denote the input-side voltage, input-side current and output voltage of the converter, respectively.

Since the proposed controller is designed in discrete time, the system model given by (9) should be discretised. Then, the discrete-time equivalent of (9) can be obtained by using the Euler's discretisation as given below:

$$I_{\text{in}}(k+1) = \frac{T}{L}(V_{\text{in}}(k) - V_0(k)\bar{u}) + I_{\text{in}}(k) \tag{10a}$$

$$V_0(k+1) = \frac{T}{C}\left(I_{\text{in}}(k)\bar{u} - \frac{V_0(k)}{R}\right) + V_0(k) \tag{10b}$$

$$V_{\text{in}}(k) = \alpha V_0(k) \tag{10c}$$

where T is the constant sampling period.

In this study, the input-voltage tracking error of the BC is defined as follows:

$$e(k) = V_{\text{in}}(k) - V_{in\_r}(k) \tag{11}$$

where $V_{\text{in}}(k)$ and $V_{in\_r}(k)$ denote the instant and reference value of the input-side rectified voltage of the BC, respectively. By using the relations given in (10c) and (11), the input-voltage tracking error can also be written in terms of the output voltage as follows:

$$e(k) = \alpha V_{\text{o}}(k) - V_{in\_r}(k) \tag{12}$$

Based on the error in (12), the sliding function for the DITSMC is defined as below [31]:

$$s(k) = s_p e(k) + s_i E(k-1) \tag{13}$$

where $s_p > 0$ and $s_i > 0$ are constant sliding-function coefficients and the integral term, $E(k)$, is defined as below:

$$E(k) = \sum_{i=0}^{k} e(i)^{\gamma} = E(k-1) + e(k)^{\gamma} \tag{14}$$

where p and q are chosen as odd integers providing that $0 < \gamma = (p/q) < 1$ to ensure the sign of the error remains intact. The $0 < \gamma < 1$ term provides a faster convergence-rate than a conventional discrete-time ISMC in which $\gamma = 1$ [31].

In this study, the DITSMC control law is designed based on the equivalent control strategy [37] as follows:

$$\Delta s = s(k+1) - s(k) = 0 \tag{15}$$

Considering (10), (12), (13) and (15), the equations given in (16) can be generated. Then, the equivalent control $u(k)$ given in (17) can be solved from (16d)

$$s(k+1) = s(k) \tag{16a}$$

$$\mapsto s_p e(k+1) + s_i E(k) = s(k) \tag{16b}$$

$$\mapsto s_p(\alpha V_o(k+1) - V_{in\_r}(k+1)) + s_i E(k) = s(k) \tag{16c}$$

$$s_p\alpha\left(\frac{T}{C}I_{in}(k)\bar{u} - V_o(k)\left(\frac{T}{RC} - 1\right)\right) - s_p V_{in\_r}(k+1) + s_i E(k) = s(k) \tag{16d}$$

$$u(k) = 1 + \left(\frac{C}{T} - \frac{1}{R}\right)\frac{V_o(k)}{I_{in}(k)} - \frac{1}{\alpha}\frac{C}{T}\frac{V_{in-r}(k+1)}{I_{in}(k)} + \frac{s_i}{s_p}\frac{1}{\alpha}\frac{C}{T}\frac{1}{I_{in}(k)}s(k) \tag{17}$$

$$e(k+1) = \alpha V_o(k+1) - V_{in\_r}(k+1) = \alpha\left(\frac{T}{C}I_{in}(k)\bar{u} - V_o(k)\left(\frac{T}{RC} - 1\right)\right) - V_{in\_r}(k+1) \tag{18}$$

In practice, the reference value of the input voltage will be defined by the used MPPT algorithm and thus $V_{in-r}(k+1)$ in given in (17) is known in prior.

3.1 Error bound and stability analysis

Considering (10b) and given in (12), the error dynamics of the closed-loop control system can be expressed as in (18).

Substituting the control-law (17) into (18), it yields that

$$e(k+1) = \frac{s(k)}{s_p} - \frac{s_i}{s_p}E(k) \tag{19}$$

and finally

$$e(k+1) = e(k) - s_{ip}e(k)^{\gamma} \tag{20}$$

where $s_{ip} = s_i/s_p$. The (20) has the same form as in (8) [38, 39]. And then, by proposition 2 given in [39], it can be proven that the error dynamics (20) will converge to a stable period-2 orbit bounded by Δ_e regardless of the initial value of the error $e(0)$. Where

$$\frac{\Delta_e}{2} = \pm\left(\frac{s_{ip}}{2}\right)^{1/(1-\gamma)} \tag{21}$$

The coefficients s_{ip} and γ do not only determine the error-bound but also determine the convergence-rate of the error. Therefore, a trial-and-error tuning process can be used to determine the sliding-function coefficients, s_{ip} and γ. The effect of s_{ip} and γ on the error dynamic is examined by simulation studies and the results are given in Fig. 5.

The rigorous theoretical analysis and proofs of the discrete-time terminal sliding mode controller design were given in detail in [38–40].

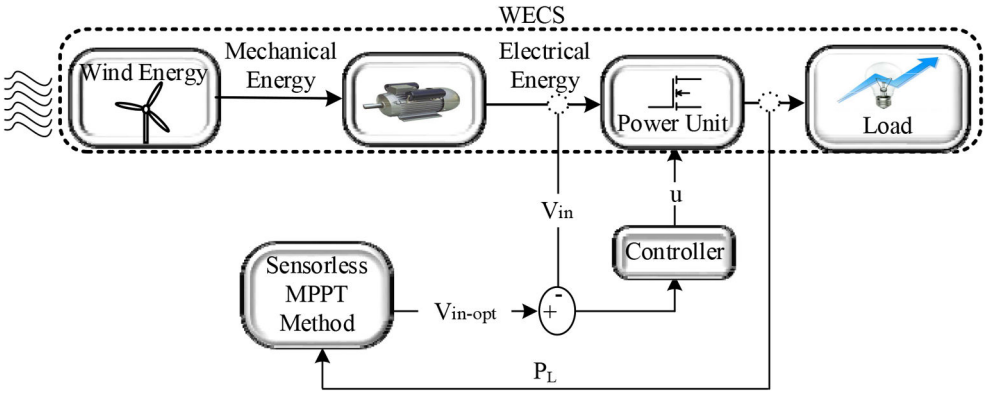

Fig. 4 *Schematic block diagram of used MPPT method*

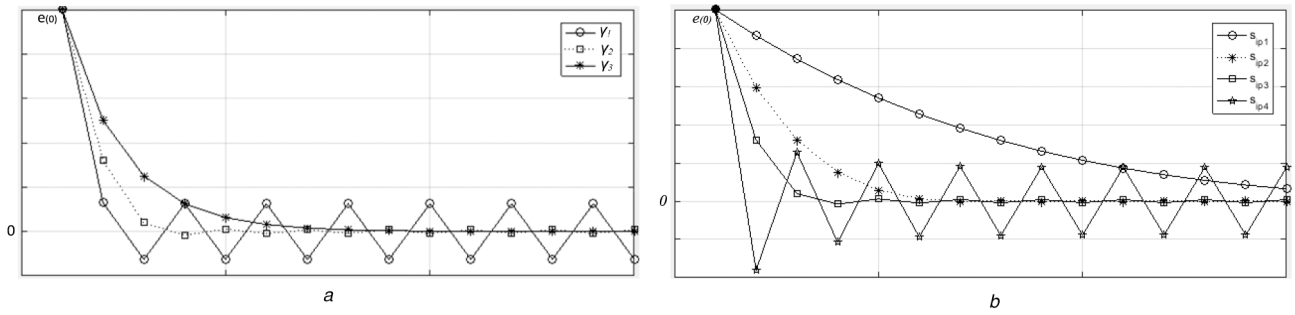

Fig. 5 *Simulation results of the sliding-function coefficients*
(a) $0 < \gamma_1 < \gamma_2 < \gamma_3 = 1$, ***(b)*** $0 < s_{ip1} < s_{ip2} < s_{ip3} < s_{ip4} = 1$

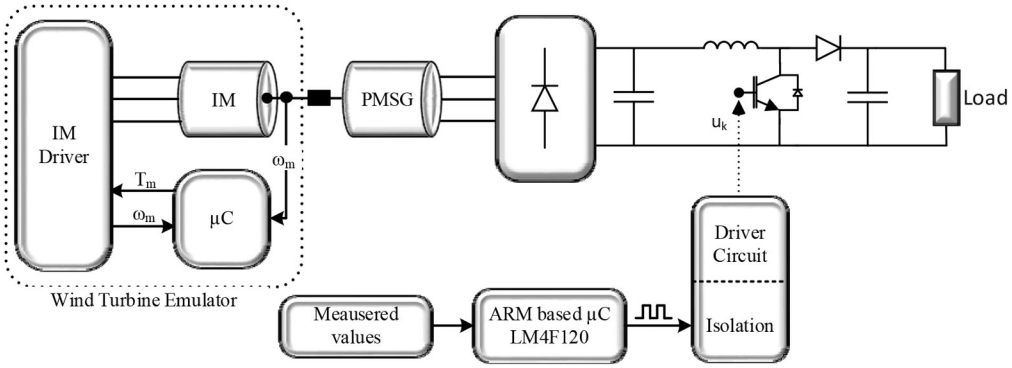

Fig. 6 *Block diagram of the WECS and the established test setup of the WECS in the laboratory, respectively*

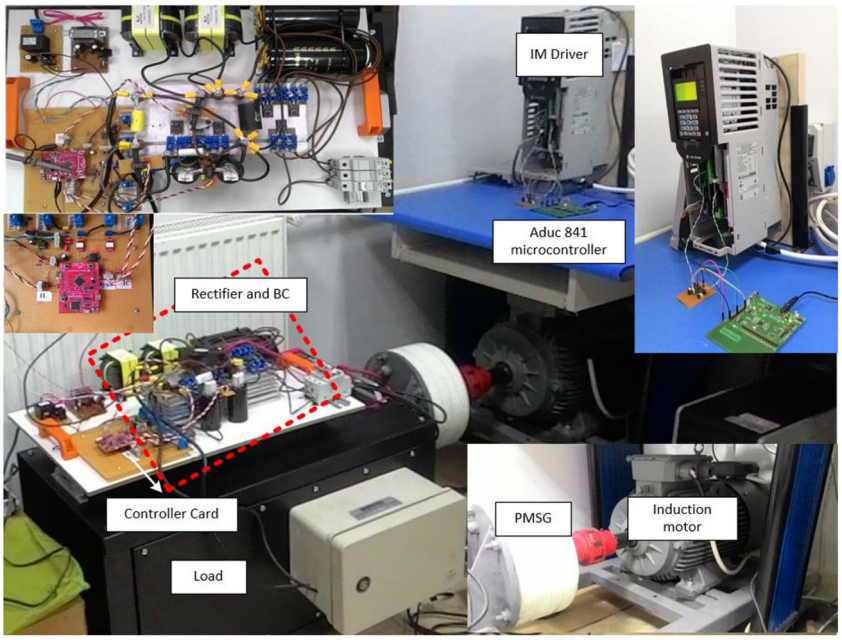

Fig. 7 *Picture of the established test setup of the WECS in the laboratory*

4 Experimental results

The block diagram and the real-time picture of the test setup established for the experimental studies are given in Figs. 6 and 7, respectively.

The performance of the proposed DITSMC-based MPPT structure is evaluated experimentally by using this test setup. As shown in Fig. 7, a WT emulator consists of a microcontroller, an induction motor (IM) and an IM driver. The reference torque signal (T_m) required for the IM driver is calculated and generated by the microcontroller (ADUC 841 in Fig. 7) depending on the wind speed and the rotational speed of the PMSG, by using the following equations:

$$\omega_{pu} = \omega/3784 \tag{22}$$

$$\lambda = \frac{8.1\omega_{pu}}{V_{w-pu}} \tag{23}$$

$$T_m = \left[\frac{\left(\frac{125.08 - 7.239\lambda}{\lambda} - 8.915\right)x}{e^{-((21-0.735\lambda)/\lambda)} + 0.01417\lambda}\right](V_{w-pu})^3 \tag{24}$$

The output voltage of the generator is rectified by the full-bridge rectifier and then delivered to the load through the BC. The proposed method is applied to the controller card (LM4F120 an ARM-based microcontroller), and so the MPPT can be achieved by changing the duty ratio of the converter. The parameters of the experimental setup are given in Table 1.

Table 1 Parameters of the experimental setup

Description	Parameter	Nominal value
input-side capacitance	C_{in}	4400 µF
inductance	L	4 mH
output capacitance	C	750 µF
load resistance	R	150 Ω
nominal power of PMSG	P_g	1.8 kW
nominal power of IM	P_m	4 kW
switching frequency	f_s	5 kHz

The sliding function coefficients are set as $s_{ip} = 0.5$ and $\gamma = 7/9$ considering the results given in Section 3.1.

In the first experiment, the controller is activated with delay to show its effect. At the beginning, the controller is off, and in this case, the WT emulator naturally accelerates and c_p has moved away from its maximum value as shown in Fig. 8*a*. As stated before, c_p indicates how close the WECS to its MPP. Therefore, it can be said that the MPPT cannot be provided if c_p deviates from its maximum value. Figs. 8*a* and *b* show the performance of the DITSMC for the constant wind speed at $V_w = 9$ m/s in case of the controller on/off states.

As it can be seen from Fig. 8, when the controller is activated, the c_p reaches its maximum value. This means that the MPPT is achieved and the efficiency of the WECS is increased.

Fig. 9 shows the performance of the DITSMC at the step-type change of the wind speed from 9 to 10 m/s. Because the controller is 'off' state, V_{in} is equal to the V_o and c_p is away from its

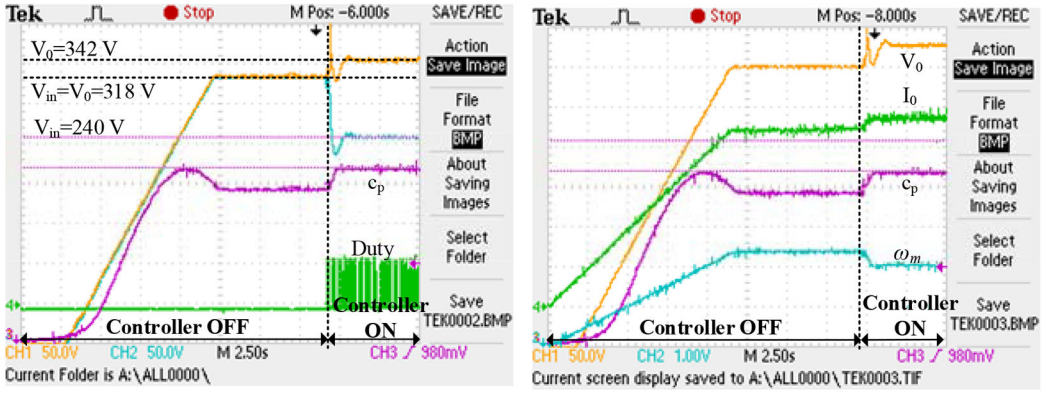

a *b*

Fig. 8 *Experimental results of the V_o, V_{in}, c_p, ω_m, I_0 and duty for on–off states of the controller at the V_w = 9 m/s*

(a) V_o, V_{in}, c_p, and duty, controller is 'off'and then 'on', ***(b)*** V_o, I_0, c_p, and ω_m, controller is 'off'and then 'on'

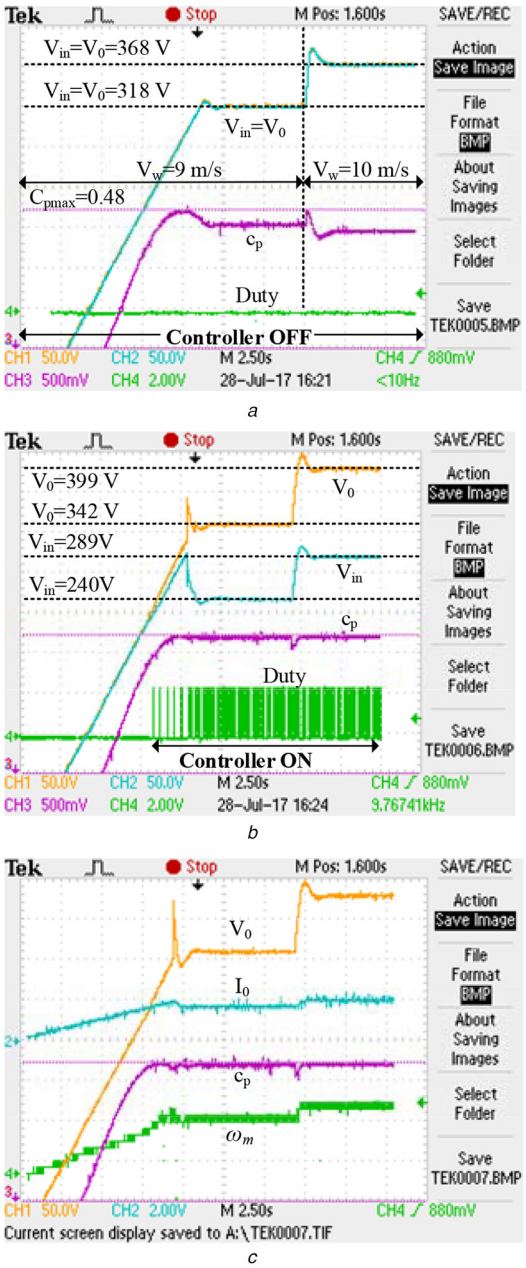

a *b* *c*

Fig. 9 *Experimental results at the step-changing wind speed from V_w = 9 to 10 m/s*

(a) V_o, V_{in}, c_p, and duty, the controller is 'off', ***(b)*** V_o, V_{in}, c_p, and duty the controller is 'on', ***(c)*** V_o, I_0, c_p, and ω_m the controller is 'on'

maximum value in Fig. 9*a*. Fig. 9*b* indicates the variations of the V_o, V_{in}, and c_p when the DITSMC is set to 'on' state. It can be seen from Fig. 9 that V_{in} assured its optimum value and thus c_p is maximised for both the wind speed 9 and 10 m/s. Additionally, I_0

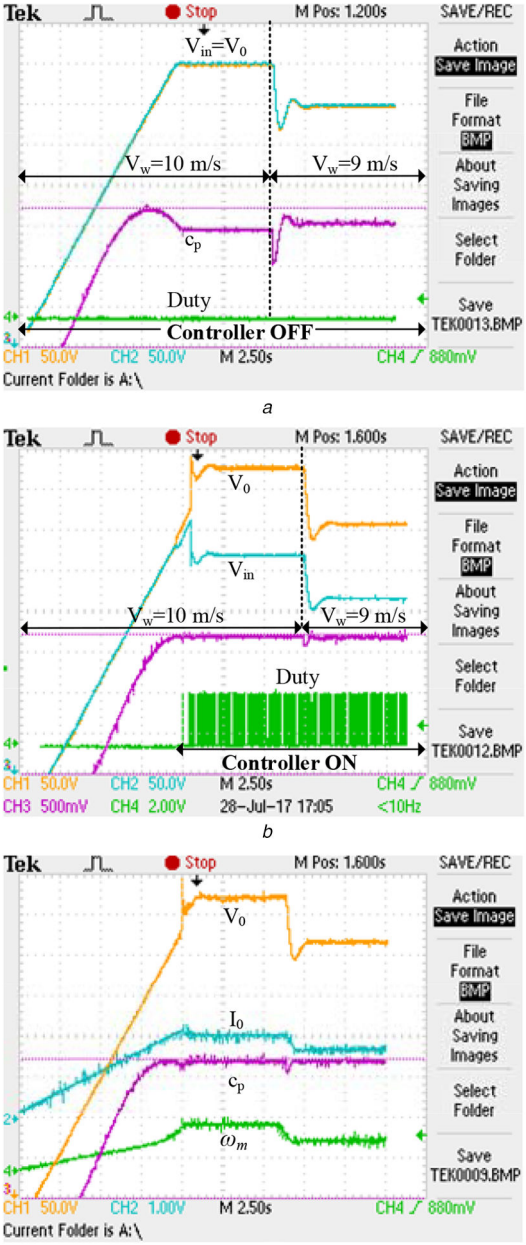

Fig. 10 *Experimental results at the step-changing wind speed from V_w = 10 to 9 m/s*

(a) V_o, V_{in}, c_p, and duty, the controller is 'off', ***(b)*** V_o, V_{in}, c_p, and duty, the controller is 'on', ***(c)*** V_o, I_0, c_p, and ω_m, the controller is 'on'

Table 2 Effect of the controller to the WECS in terms of the efficiency

V_w, m/s	Controller-off			Controller-on		
	V_{in}, V	P_L, W	WECS efficiency, %	V_{in}, V	P_L, W	WECS efficiency, %
9	318	674	81.62	240	779	≃94.40
10	368	902	84.64	289	1061	≃99.50

and ω_m are analysed in Fig. 9*c*. The controller brings the WECS to the MPPT ∼550 ms when the wind speed changes from 9 to 10 m/s.

Fig. 10 shows the performance of the DITSMC controller when the wind speed changes from 10 to 9 m/s. It is clear from Figs. 10*b* and *c* that the MPPT is achieved when the controller is activated. Moreover, the MPPT is achieved again ∼500 ms even if the wind speed is suddenly down from 10 to 9 m/s.

The effect of the proposed MPPT structure to the WECS in terms of the efficiency is tabulated and given in Table 2.

The last experimental study is the comparison of the performances of the PI and DITSMC controllers given in Fig. 11. The PI controller parameters were set as $k_p = 0.155$ and $k_i = 0.065$, considering the overshoot and settling time. In Fig. 10*a*, the performance of the PI controller is presented.

The settling-time of the PI controller is ∼1.25 s while the settling time of the proposed controller is ∼550 ms. On the other hand, both controllers perform approximately the same performance in terms of the overshoot criteria. Therefore, it is proved from the experimental study that the performance of the proposed DITSMC is better than the PI controller in terms of the settling time and thus, the efficiency of the WECS.

5 Conclusion

In this study, the DITSMC-based MPPT structure was proposed to increase the energy efficiency of a WECS by decreasing the

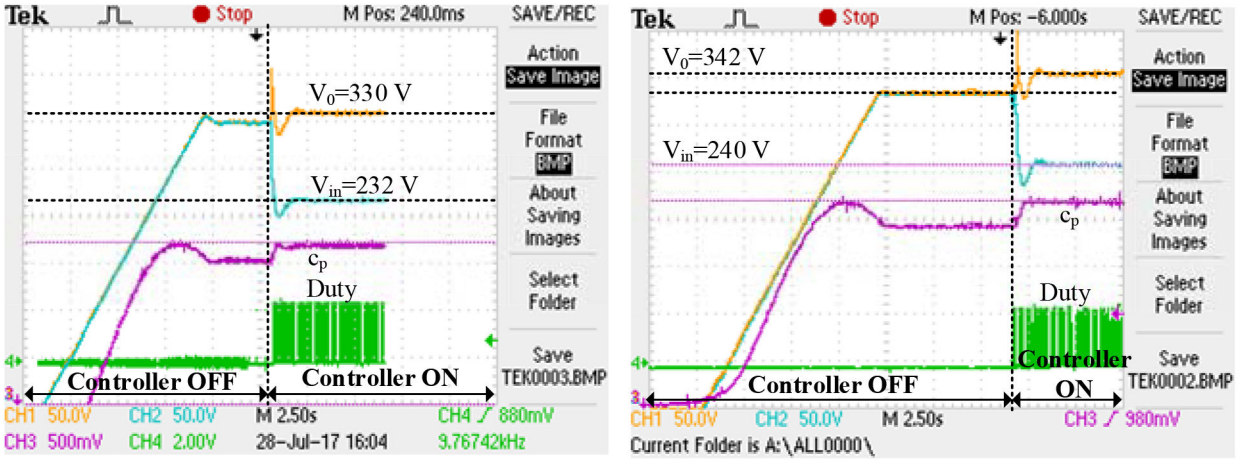

Fig. 11 *Experimental results of the V_o, V_{in}, c_p, and duty at V_w = 9 m/s*
(a) PI controller, ***(b)*** DITSMC controller

convergence-time and the error-bound around the MPP determined by the PSF-based algorithm. The effects of the design parameters of the DITSMC on the convergence-time and the error-bounds were investigated by the simulation studies. The dynamic performance of the proposed DITSMC was proved with the experiments on a test setup for various wind conditions. Through the proposed method, the maximum power value obtained from WECS was increased by up to 15%. In addition, the performance of the proposed DITSMC is compared with the PI controller under the same conditions. It is proved from the experimental studies that the DITSMC has better performance than the PI controller in terms of settling time and thus the efficiency of the WECS.

6 References

[1] Huang, C., Li, F., Jin, Z.: 'Maximum power point tracking strategy for large-scale wind generation systems considering wind turbine dynamics', *IEEE Trans. Ind. Electron.*, 2015, **62**, (4), pp. 2530–2539

[2] Calderaro, V., Galdi, V., Piccolo, A., *et al.*: 'A fuzzy controller for maximum energy extraction from variable speed wind power generation systems', *Electr. Power Syst. Res.*, 2008, **78**, (6), pp. 1109–1118

[3] Masoud Barakati, S.: 'Modeling and controller design of a wind energy conversion system including a matrix converter'. PhD Thesis, University of Waterloo, 2008

[4] Eltamaly, A.M., Farh, H.M.: 'Maximum power extraction from wind energy system based on fuzzy logic control', *Electr. Power Syst. Res.*, 2013, **97**, pp. 144–150

[5] Wang, Q., Chang, L.: 'An intelligent maximum power extraction algorithm for inverter-based variable speed wind turbine systems', *IEEE Trans. Power Electron.*, 2004, **19**, (5), pp. 1242–1249

[6] Lee, J., Kim, Y.: 'Sensorless fuzzy-logic-based maximum power point tracking control for a small-scale wind power generation systems with a switched-mode rectifier', *IET Renew. Power Gener.*, 2016, **10**, (2), pp. 194–202

[7] Mancilla-David, F., Ortega, R.: 'Adaptive passivity-based control for maximum power extraction of stand-alone windmill systems', *Control Eng. Pract.*, 2012, **20**, (2), pp. 173–181

[8] Aissaoui, A.G., Tahour, A., Essounbouli, N., *et al.*: 'A fuzzy-PI control to extract an optimal power from wind turbine', *Energy Convers. Manage.*, 2013, **65**, pp. 688–696

[9] Wang, Y., Chen, R., Tan, J., *et al.*: 'An optimal PID control of wind generation based on matrix converter'. IEEE Int. Power Electronics and Motion Control Conf., Wuhan, China, 2009, pp. 1104–1109

[10] Sheikhan, M., Shahnazi, R., Nooshad Yousefi, A.: 'An optimal fuzzy PI controller to capture the maximum power for variable-speed wind turbines', *Neural Comput. Appl.*, 2013, **23**, (5), pp. 1359–1368

[11] Fatih Kececioglu, O., Acikgoz, H., Yildiz, C., *et al.*: 'Power quality improvement using hybrid passive filter configuration for wind energy systems', *J. Electr. Eng. Technol.*, 2017, **12**, (1), pp. 207–216

[12] Merida, J., Aguilar, L.T., Jorge, D.: 'Analysis and synthesis of sliding mode control for large scale variable speed wind turbine for power optimization', *Renew. Energy*, 2014, **71**, pp. 715–728

[13] Chen, J.-H., Yau, H.-T., Hung, W.: 'Design and study on sliding mode extremum seeking control of the chaos embedded particle swarm optimization for maximum power point tracking in wind power systems', *Energies*, 2014, **7**, (3), pp. 1706–1720

[14] Yin, X., Lin, Y., Li, W., *et al.*: 'Sliding mode voltage control strategy for capturing maximum wind energy based on fuzzy logic control', *Electr. Power Energy Syst.*, 2015, **70**, pp. 45–51

[15] Weng, Y.-T., Hsu, Y.-Y.: 'Sliding mode regulator for maximum power tracking and copper loss minimisation of a doubly fed induction generator', *IET Renew. Power Gener.*, 2015, **9**, (4), pp. 297–305

[16] Beltran, B., Ahmed-Ali, T., Benbouzid, M.E.H.: 'High-order sliding-mode control of variable-speed wind turbines', *IEEE Trans. Ind. Electron.*, 2009, **56**, (9), pp. 3314–3321

[17] Slotine, H.-J.E., Li, W.: '*Applied nonlinear control*' (Prentice-Hall, USA, 1991)

[18] Utkin, V.I.: 'Sliding mode control design principles and applications to electric drives', *IEEE Trans. Ind. Electron.*, 1993, **40**, (1), pp. 23–36

[19] Young, K.D., Utkin, V.I., Özgüner, Ü.: 'A control engineer's guide to sliding mode control', *IEEE Trans. Control Syst. Technol.*, 1999, **7**, (3), pp. 328–342

[20] Özbay, H., Öncü, S., Kesler, M.: 'SMC-DPC based active and reactive power control of grid-tied three phase inverter for PV systems', *Int. J. Hydrog. Energy*, 2017, **42**, (28), pp. 17713–17722

[21] Diab, M.S., Elserougi, A., Abdel-Khalik, A.S., *et al.*: 'Four-switch three-phase SEPIC-based inverter', *IEEE Trans. Power Electron.*, 2015, **30**, (9), pp. 4891–4905

[22] Tan, S.C., Lai, Y.M., Tse, C.K.: 'Indirect sliding mode control of power converters via double integral sliding surface', *IEEE Trans. Power Electron.*, 2008, **23**, (2), pp. 600–611

[23] Zhao, H., Wu, Q., Rasmussen, C.N., *et al.*: 'L1 adaptive speed control of a small wind energy conversion system for maximum power point tracking', *IEEE Trans. Energy Convers.*, 2014, **29**, (3), pp. 576–584

[24] Utkin, V., Shi, J.S.J.: 'Integral sliding mode in systems operating under uncertainty conditions'. Proc. of 35th IEEE Conf. on Decision and Control, Kobe, Japan, 1996, pp. 4591–4596

[25] Chiu, C.-S., Ouyang, Y.-L., Ku, C.-Y.: 'Terminal sliding mode control for maximum power point tracking of photovoltaic power generation systems', *Sol. Energy*, 2012, **86**, (10), pp. 2986–2995

[26] Venkataraman, S.T., Gulati, S.: 'Control of nonlinear systems using terminal sliding modes', *J. Dyn. Syst. Meas. Control*, 1993, **115**, (3), pp. 554–560

[27] Mondal, S., Mahanta, C.: 'Adaptive second order terminal sliding mode controller for robotic manipulators', *J. Franklin Inst.*, 2014, **351**, (4), pp. 2356–2377

[28] Pan, Y., Yang, C., Pan, L., *et al.*: 'Integral sliding mode control: performance, modification and improvement', *IEEE Trans. Ind. Inf.*, 2018, **14**, (7), pp. 3087–3096

[29] Ullah, N., Ali, M.A., Ibeas, A., *et al.*: 'Adaptive fractional order terminal sliding mode control of doubly fed induction generator based wind energy system', *IEEE Access*, 2017, **5**, pp. 21368–21381

[30] Ebrahimkhani, S.: 'Robust fractional order sliding mode control of doubly-fed induction generator (DFIG)-based wind turbines', *ISA Trans.*, 2016, **63**, pp. 343–354

[31] Xu, Q.: 'Digital integral terminal sliding mode predictive control of piezoelectric-driven motion system', *IEEE Trans. Ind. Electron.*, 2016, **63**, (6), pp. 3976–3984

[32] Heier, S.: '*Grid integration of wind energy conversion systems*' (John Wiley & Sons, UK, 1998)

[33] Gitano-Briggs, H.: 'Small wind turbine power controllers', in Muyeen, S.M. (Ed.): '*Wind power*' (Intech, Croatia, 2010), pp. 165–188

[34] Fitzgerald, A.E., Kingsley, C.J., Umans, S.D.: '*Electric machinery*' (McGraw Hill, USA, 2005, 6th edn.)

[35] Abdullah, M.A., Yatim, A.H.M., Tan, C.W., *et al.*: 'A review of maximum power point tracking algorithms for wind energy systems', *Renew. Sustain. Energy Rev.*, 2012, **16**, (5), pp. 3220–3227

[36] Yin, X.-X., Lin, Y.-G., Li, W., *et al.*: 'Fuzzy-logic sliding-mode control strategy for extracting maximum wind power', *IEEE Trans. Energy Convers.*, 2015, **30**, (4), pp. 1267–1278

[37] Xu, Q., Li, Y.: 'Micro-/nanopositioning using model predictive output integral discrete sliding mode control', *IEEE Trans. Ind. Electron.*, 2012, **59**, (2), pp. 1161–1170

[38] Li, S., Du, H., Yu, X.: 'Discrete-time terminal sliding mode control systems based on Euler's discretization', *IEEE Trans. Autom. Control*, 2014, **59**, (2), pp. 546–552
[39] Yu, X., Xu, J.X., Hong, Y.*, et al.*: 'Analysis of a class of discrete-time systems with power rule', *Automatica*, 2007, **43**, (3), pp. 562–566
[40] Behera, A.K., Bandyopadhyay, B.: 'Steady-state behaviour of discretized terminal sliding mode', *Automatica*, 2015, **54**, pp. 176–181